ICIC Express Letters
Part B: Applications
Volume **10**, Number **2**, February **2019**

ICIC International ©2019 ISSN 2185-2766
pp. **175–184**

ANALYSIS OF DIAGNOSTIC FEATURES FROM FUNDUS IMAGE USING MULTISCALE WAVELET DECOMPOSITION

Mithun Kumar Kar[1], Giritharan Ravichandran[2]
Poonguzhali Elangovan[1] and Malaya Kumar Nath[1]

[1]Department of Electronics and Communication Engineering
National Institute of Technology Puducherry
Thiruvettakudy, Karaikal 609609, Puducherry, India
{ mithunkar.iitg; epoonguzhali3; malaya.nath }@gmail.com

[2]Department of Electronics and Communication Engineering
E.G.S. Pillay Engineering College
Old Nagore Road, Thethi Village, Nagapattinam 611002, Tamil Nadu, India
giritharan101995@gmail.com

Received September 2018; accepted November 2018

Abstract. *Different diagnostic features such as microaneurysms, hemorrhages, and exudates appear over the retina due to diabetic retinopathy (DR) and cause vision loss. Analysis of fundus image plays a vital role in monitoring and diagnosis of different allied diseases due to DR. In this paper, multiscale analysis of diagnostic features has been studied in different wavelet subbands. Feature information is analyzed in different subbands for 3-, 5-, 7- and 9-level of wavelet decomposition. From the analysis, it reveals that the different wavelet subbands carry different information about the retinal feature. Analysis of retinal features is performed on DRIVE, ARIA and Messidor databases and the performance is determined by using statistical measures such as accuracy, sensitivity, and specificity. The experimental study shows that the diagnostic feature information is distributed over different wavelet subbands for a particular level of wavelet decomposition. Microaneurysm information is mainly present in higher wavelet subbands compared to lower wavelet subbands. Exudates information is present in some subbands. In other words, it may be represented as few subbands do not contain any significant information about the diagnostic feature. Subbands containing less diagnostic information can be omitted for further analysis. This will help in efficient classification, segmentation and detection purposes.*

Keywords: Retinal image, Wavelet decomposition, Microaneurysms, Exudates, Diabetic retinopathy (DR)

1. **Introduction.** Diabetic retinopathy (DR) is a chronic disease related to eye where the retina is progressively damaged and causes vision loss [1]. According to the World Health Organization (WHO) report, the people having diabetics will increase to nearly 300 million by the year 2025 [2], which can be controlled if analyzed at the early stage by a retinal screening test. The important diagnostic features over the normal retina are optic disc, fovea and blood vessels. Different diagnostic features emerge over the retina due to DR such as microaneurysms (MAs), hemorrhages, and exudates, which gradually damages the retina [3]. Microaneurysm is the first clinically observable lesions appearing as red tiny round dots near the blood vessels which have a similar contrast to that of the blood vessels pixels. As the disease progresses hemorrhages appear over the retina [4]. Exudates are the brightest feature similar to the optic disc which comes out of the damaged blood vessels and they are the clinical symptoms of the related disease like retinal venous obstruction, radiation retinopathy, Coat's disease, capillary hemangioma

DOI: 10.24507/icicelb.10.02.175

of the retina, macular edema, and hypertensive retinopathy including DR [5]. Diabetic macular edema (DME) is a most common disease due to exudates and it has three severity levels, such as mild, moderate and severe depending on the diagnostic feature distribution and distance from the fovea centre [6].

Usually, ophthalmologists look to the appearance and position of the features to diagnose vision loss. Extra care must be taken to avoid the loss of diagnostic components in the fundus images during the analysis [7]. A good number of papers are present in the literature about the segmentation of the pathological features from the color fundus images. However, a limited number of papers have been published in the literature for the study of diagnostic features in different wavelet subbands. The main objective of the present work is to analyze the pathological features at different wavelet subbands for the purpose of segmentation, analysis, and classification. This analysis is studied by a discrete wavelet transform (DWT), which has the property of multiresolution or multiscale. Due to this property of DWT, the feature which is difficult to be detected at one scale may be easily detected by another scale. Nirmala et al. [8] find the anatomical structure of the blood vessels information in different wavelet subbands. The thick and thin blood vessels are distributed in the different resolution of the DWT. Large blood vessels are extracted by low-resolution images, whereas thin and fine blood vessels are extracted by high-resolution images.

Quality assessment should be done in medical images for quality diagnosis. Fundus image contains the diagnostic feature which has to be considered and the nondiagnostic information is to be ignored. The objective of the present work is to study the distribution of diagnostic feature across different wavelet subbands. Multiresolution or multiscale property of DWT provides features that are difficult to detect at one scale may be detected at other scales. Multiresolution analysis helps to produce localized image features with good space frequency resolution. Fundus images contain fine anatomical feature (such as blood vessels and exudates) and slowly varying feature (optic disc, hemorrhages, and background). Pathological features such as microaneurysms, hemorrhages. and exudates contain the diagnostic information about the condition of vision. In this proposed method, the subband containing higher diagnostic information is determined by both the subjective and objective measures. Subjective measures are more reliable and time-consuming. Different objective quality measures (such as sensitivity, specificity, sensibility, accuracy, equal error rate, mean square error (MSE), root mean square error (RMSE), mean absolute error (MAE), Pearson correlation coefficient (PCC), universal quality index (UQI) and structural similarity index (SSIM)) are used to analyze the contribution of different subbands towards the diagnostic information [9, 10].

A novel method is used for the analysis of the pathological features in different wavelet subbands by 2D DWT, where different levels of wavelet decomposition are performed using Daubechies-4 mother wavelet on the green channel of the color fundus image as it has higher contrast between the background and the features. In each level of decomposition, the images are reconstructed by considering the approximate subband coefficients at the final level and one detail subband coefficients at a time. From each reconstructed image the diagnostic feature is analyzed. The rest of the paper is organized as follows. The proposed method for analysis of the diagnostic features is discussed in Section 2. In Section 3 results are discussed. Conclusions are given in Section 4.

2. **Proposed Method.**

The important aspect of medical images is the information of interest which is spatially localized. Multiscale transform is the most popular multiresolution analysis (MRA) technique, which segregates the information of an image into a different wavelet subband matrix depending on the frequency [11]. In 2D DWT, the image is decomposed into one low-frequency approximation (A) subband and three high-frequency detailed subbands such as horizontal (H) subband, vertical (V) subband, and

diagonal (D) subband. The scaling and wavelet function in 2D at a resolution level i can be represented by

$$\phi_{i,m,n}(x,y) = 2^{i/2}\phi(2^i x - m, 2^i y - n) \tag{1}$$

$$\psi^b_{i,m,n}(x,y) = 2^{i/2}\psi^b(2^i x - m, 2^i y - n) \tag{2}$$

where b represents the detail subbands H, V, and D. The DWT of an image $p(x,y)$ of size $(P \times Q)$ can be defined as:

$$WT_\phi(i_0,m,n) = \frac{1}{\sqrt{PQ}} \sum_{x=0}^{P-1}\sum_{y=0}^{Q-1} p(x,y)\phi_{i_0,m,n}(x,y) \tag{3}$$

$$WT^b_\psi(i,m,n) = \frac{1}{\sqrt{PQ}} \sum_{x=0}^{P-1}\sum_{y=0}^{Q-1} p(x,y)\psi^b_{i,m,n}(x,y) \tag{4}$$

where i_0 is an arbitrary starting level/scale and the $WT_\phi(i_0,m,n)$ coefficients define approximation of $p(x,y)$ at scale i_0. Here, (m,n) determines the position of wavelet function. The $WT^b_\psi(i,m,n)$ defines horizontal, vertical, and diagonal details for scales $i \geq i_0$. Given WT_ϕ and WT^b_ψ of Equation (3) and Equation (4), $p(x,y)$ is obtained via inverse DWT as:

$$\begin{aligned} p(x,y) = {} & \frac{1}{\sqrt{PQ}} \sum_m \sum_n WT_\phi(i_0,m,n)\phi_{i_0,m,n}(x,y) \\ & + \frac{1}{\sqrt{PQ}} \sum_{b=H,V,D} \sum_{i\geq i_0} \sum_m \sum_n WT^b_\psi(i,m,n)\psi^b_{i,m,n}(x,y) \end{aligned} \tag{5}$$

An N-level DWT gives rise to $(3N+1)$ subbands, one approximation band at the final level of decomposition and three detail bands (H, V, and D) at each level of decomposition. The coefficients of approximation band and the detail bands of each level form the feature vector or decomposition vector $[A(N), H(N), V(N), D(N), H(N-1), V(N-1), D(N-1), \ldots, H(1), V(1), D(1)]$.

In this paper 3-, 5-, 7-, and 9-level of wavelet decomposition are performed by Daubechies-4 (dB4) mother wavelet on the green channel to study the diagnostic information of the pathological features from the color fundus images. The dB4 is nearly symmetric compared to dB2. Daubechies-4 mother wavelet is orthogonal and has finite vanishing moments [12]. This property ensures that the number of non-zero coefficients in the associated filter is finite. This is very useful for local analysis. It closely matches to the signal to be processed. So, dB4 is suitable for biomedical images and signal processing applications [13]. The different levels of wavelet decomposition on the fundus images generate one approximation band at final level and 9, 15, 21, 27 number of detail bands at 3-, 5-, 7-, and 9-level wavelet decomposition, respectively. As each subband contains the anatomical and pathological feature information from the diagnostic point of view, it is important to know the significance of each subband in each level of decomposition. This analysis of feature information in different subbands for different levels of decomposition is performed in two ways. In the first case, the detail subband coefficients of one level are altered at a time without unaltering the other detail subband coefficients. In the second case, one of the detail subband coefficients are unaltered by altering the rest of the subband coefficients.

2.1. **Analysis of microaneurysms and hemorrhages in wavelet subbands.** In this subsection, the pathological features such as microaneurysms and hemorrhages are analyzed in different subbands of 3-, 5-, 7- and 9-level of wavelet decomposition by dB4 mother wavelet. In the green channel image, they appear as darker spots compared to the background. Hemorrhages appear as red cluster/patches in the retinal image. They look like a darker patch. Hemorrhages and microaneurysms are similar in color to that of

the blood vessel. Before finding the feature information they are cropped from the other regions of the retinal image to have a detail information. The microaneurysm feature is cropped from the green channel image, as this channel is moderately saturated compared to the blue channel and red channel image. Different levels of wavelet decompositions are applied to this image for multiresolution analysis (MRA) of the microaneurysms information in different wavelet subbands.

Three level (3-level) wavelet decomposition process generates one approximation band at the third level of decomposition and three detail subbands at each level ($L1$ ($H1$, $V1$, $D1$), $L2$ ($H2$, $V2$, $D2$), and $L3$ ($H3$, $V3$, $D3$)). To illustrate the importance of subbands at each decomposition level the images are reconstructed after zeroing/altering the coefficients of one level at a time or unaltering the coefficients of any one level at a time. The reconstructed images are shown in Figure 1. Figure 1(a) is the high contrast DR fundus image, whereas Figure 1(b) is the reconstructed image. The final level approximation band image is shown in Figure 1(c). The features appear to be similar in these reconstructed images. Figure 1(d), Figure 1(e) and Figure 1(f) are the reconstructed images after zeroing the coefficients of $L1$ ($H1$, $V1$, $D1$), $L2$ ($H2$, $V2$, $D2$), and $L3$ ($H3$, $V3$, $D3$) subbands, respectively. Figure 1(g), Figure 1(h) and Figure 1(i) are the images reconstructed after unaltering the coefficients of $L1$, $L2$, and $L3$ subbands, respectively, whereas other subbands coefficients are made zero. It is observed that the diagnostic features are well reconstructed in three level wavelet decomposition and hence the overall image quality is good compared to the original image.

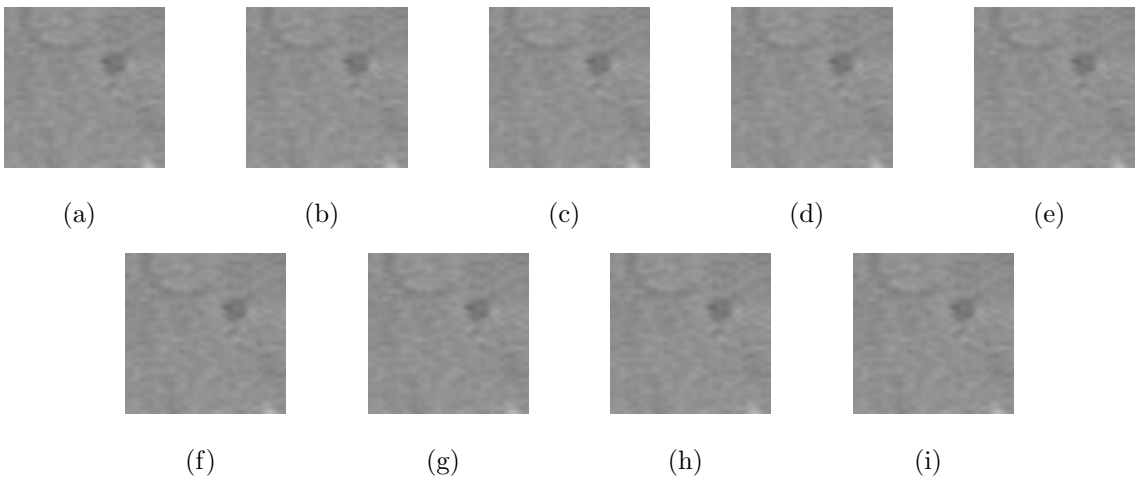

FIGURE 1. Microaneurysm feature analysis in different subbands of 3-level wavelet decomposition: (a) high contrast green channel image, (b) reconstructed image, (c) reconstructed image considering approximation band coefficients, (d) reconstructed image zeroing $L1$ ($H1$, $V1$, $D1$) coefficients, (e) reconstructed image zeroing $L2$ ($H2$, $V2$, $D2$) coefficients, (f) reconstructed image zeroing $L3$ ($H3$, $V3$, $D3$) coefficients, (g) reconstructed image unaltering only $L1$ coefficients, (h) reconstructed image unaltering only $L2$ coefficients, (i) reconstructed image unaltering only $L3$ coefficients

For further analysis of the microaneurysms feature, the level of decomposition is increased to fifth level. Figure 2 shows analysis of different subbands in 5-level wavelet decomposition. The same procedure is followed to that of the third level wavelet decomposition. Figure 2(a) to Figure 2(e) are the reconstructed images after zeroing the coefficients of $L1$-subband to $L5$-subband, respectively. Similarly, Figure 2(f) to Figure 2(j) are the images obtained by unaltering the coefficients of $L1$-subband, $L2$-subband,

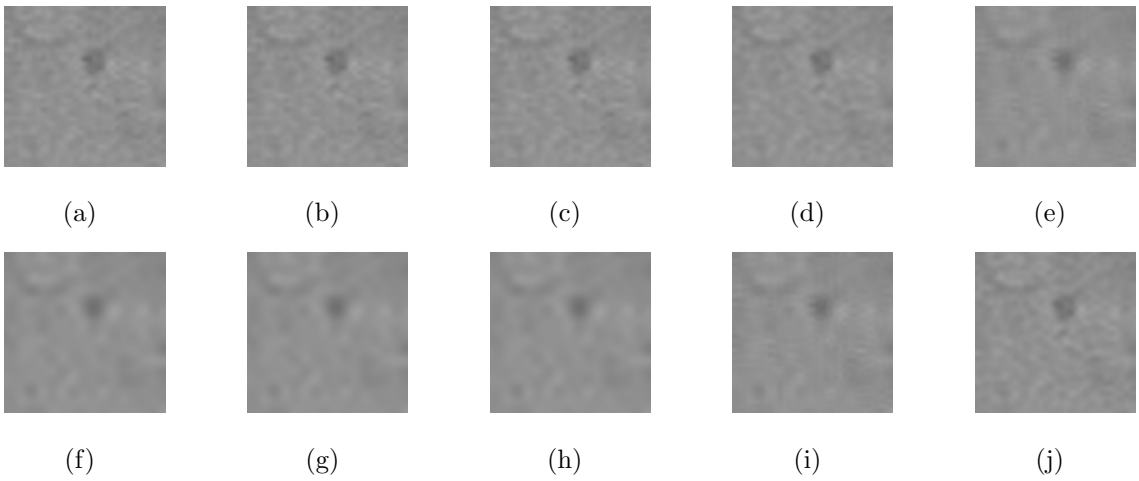

FIGURE 2. Microaneurysm feature analysis in different subbands of 5-level wavelet decomposition: (a)-(e) reconstructed images by zeroing $L1$ to $L5$ subband coefficients, (f)-(j) reconstructed images by unaltering $L1$ to $L5$ subband coefficients, respectively and altering the coefficients of other subbands

$L3$-subband, $L4$-subband, and $L5$-subband, respectively and zeroing the rest subband coefficients. From Figure 2(a), Figure 2(b) and Figure 2(c) it is clear that $L1$, $L2$, and $L3$ subband coefficients are not influencing the microaneurysm features much. The microaneurysm and the hemorrhages are affected by altering the coefficients of $L4$ and $L5$ subbands coefficients. Figure 2(d) and Figure 2(e) are the reconstructed images obtained after zeroing the coefficients of $L4$ and $L5$ subband coefficients, respectively. It is observed that the microaneurysm feature is not reconstructed properly and the overall quality of this feature is reduced. Similarly, Figure 2(f) to Figure 2(j) are reconstructed by retaining the coefficients of $L1$ to $L5$ subbands, respectively and zeroing the rest of the subband coefficients. This does not affect the reconstruction of the DR feature much when the coefficients of $L4$ and $L5$ subbands are present. The reconstructed images are shown in Figure 2(i) and Figure 2(j), respectively. The diagnostic feature is influenced when the coefficients of $L4$ and $L5$ subbands are made zero. In Figure 2(f) to Figure 2(h), the coefficients of $L4$ and $L5$ subbands are zero. So, the feature is not reconstructed properly. Retaining the coefficients of $L4$ and $L5$ subbands the quality of the DR feature in the reconstructed image is not degraded. It is observed that any alteration in subband coefficients of $L4$ and $L5$ will affect the diagnostic information in the 5-level of wavelet decomposition. It may be concluded that the coefficients of $L4$ and $L5$ subbands contribute more towards DR feature information in a five-level wavelet decomposition.

To have a better understanding of the diagnostic feature distribution (microaneurysms) in different reconstructed subbands the level of decomposition is increased (7-level and 9-level). In 7-level, it is observed that the subbands of $L5$, $L6$, and $L7$ have significant microaneurysm and hemorrhages information. It may be concluded that subbands $L5$ and $L6$ contribute more towards the microaneurysms features in 9-level wavelet decomposition compared to $L7$, $L8$, and $L9$ subbands. Thus, it is observed that the higher subbands contribute more towards diagnostic feature information for microaneurysms and hemorrhages.

2.2. **Analysis of exudates in wavelet subband.** In this subsection, exudates are analyzed in different subbands of 5-, 7- and 9-level wavelet decomposition. Exudates are more prominent diagnostic features than the microaneurysms and hemorrhages. For analysis, green channel image is used and the decomposition is performed in the same way as

that of microaneurysms and hemorrhages. Figure 3 shows the appearance of the exudates in different subbands for a five-level wavelet decomposition. In this case, the subband images are reconstructed in the same way as discussed in the previous subsection. The images shown in Figure 3(a) to Figure 3(e) are formed by altering coefficients of $L1$ to $L5$ subbands, respectively. The images shown in Figure 3(f) to Figure 3(j) are reconstructed by retaining the coefficients of one subband at a time and altering the values of other subband coefficients to zero. Subbands $L4$ and $L5$ have the blood vessel (BV) information. By altering $L4$ and $L5$ coefficients to zero, blood vessels information is reduced and the reconstructed images are shown in Figure 3(d) and Figure 3(e). The exudate information is preserved in $L1$, $L2$ and $L3$ subbands with less information about the blood vessels. In Figure 3(f), Figure 3(g), and Figure 3(h) only $L1$, $L2$ and $L3$ subband coefficients are present. It is observed that combining the coefficients of $L1$, $L2$, and $L3$ subbands, the exudate information can be preserved and the BV information can be suppressed. In Figure 4 selective subband coefficients are combined and other subband coefficients are made zero for reconstruction of the exudates. For the image shown in Figure 4(a), $L4$ and $L5$ subband coefficients are reduced to zero and $L1$, $L2$ and $L3$ subband coefficients are kept unaltered. In this case, blood vessels are seen with the exudates. For the image shown in Figure 4(b), $L1$ subband and $L2$ subband coefficients are retained with $L3$-subband,

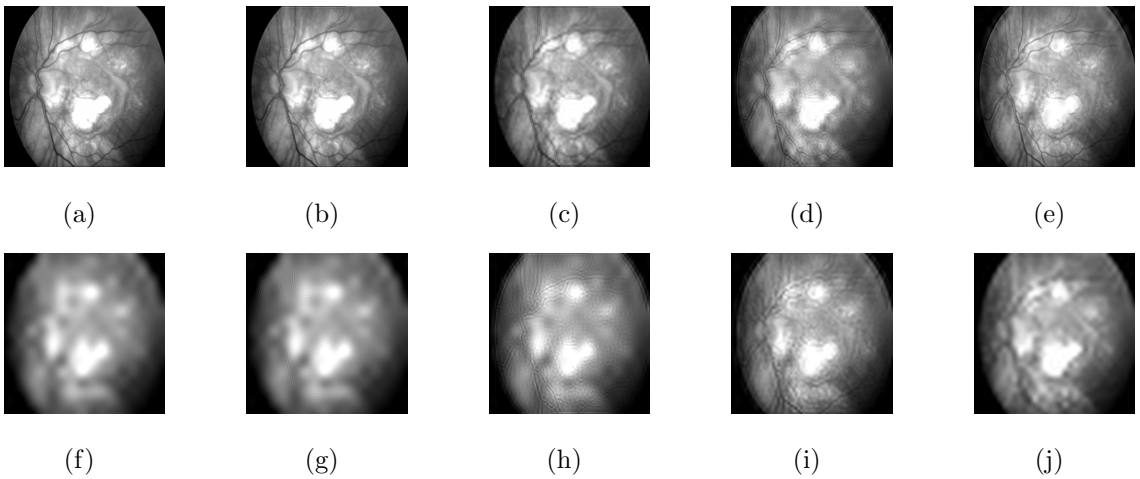

FIGURE 3. Analysis of exudates in different subbands of 5-level wavelet decomposition: (a)-(e) reconstructed images by zeroing $L1$ to $L5$ subband coefficients, respectively, (f)-(j) reconstructed images by unaltering $L1$ to $L5$ subband coefficients, respectively and altering other coefficients

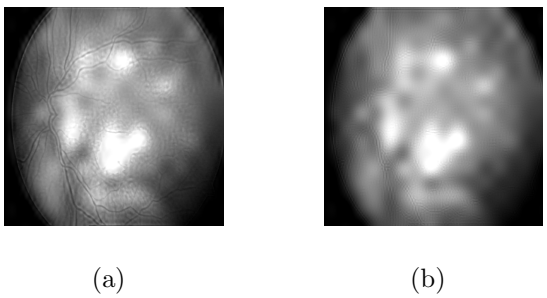

FIGURE 4. Exudates information in the combination of different subband coefficients in 5-level wavelet decomposition: (a) reconstructed image without altering $L1$, $L2$ and $L3$ subband coefficients only, (b) reconstructed image without altering $L1$ and $L2$ subband coefficients only

and $L4$-subband and $L5$-subband coefficients are made as zero. It can be observed that the exudates are preserved and the blood vessels are present with very low contrast. The quality of exudates is better compared to the other cases.

For further analysis of exudates in the wavelet subbands, the decomposition level is increased (7-level and 9-level). In 7-level wavelet decomposition, it is observed that the coefficients of $L4$, $L3$, and $L2$ subbands do not contain significant exudate information. The most important subbands contributing to exudate information are $L7$, $L6$, $L5$, and $L1$. In 9-level decomposition, it is observed that the coefficients of $L9$, $L5$, $L4$, $L3$, and $L2$ subbands do not contain significant exudate information. The most important subbands contributing to exudate information are $L8$, $L7$, $L6$, and $L1$.

3. **Quantitative Evaluation of Diagnostic Features in Wavelet Subband.** Multiscale analysis of diagnostic features (microaneurysms, hemorrhages, and exudates) is tested on DRIVE database [14], ARIA database [15], and Messidor database [16]. DRIVE database contains 40 test images, compressed in TIF format of 512×512 pixels. The 40 images are divided into test set and training set, each of which contains 20 images. For each image in test set and training set manual segmentation data is available. ARIA database contains 129 pathologically affected images, compressed in JPEG format. In this work, sensitivity (SEN) [17], specificity (SPF) [18, 19], sensibility (SEB) [20, 21], accuracy (ACC) [18, 22], equal error rate (EER), mean square error (MSE), root mean square error (RMSE) [23], peak signal to noise ratio (PSNR) [23], mean absolute error (MAE) [23, 24], Pearson correlation coefficient (PCC) [23, 24], universal quality index (UQI) [19], structural similarity (SSIM) [25, 26] are used to evaluate quantitatively the diagnostic information present in different wavelet subbands.

Microaneurysms and hemorrhages are extracted by mathematical morphology based method from the original image and the reconstructed image is obtained by 5-level and 7-level wavelet decomposition. The green channel of the fundus image is considered and the image is resized to 512×512. The resized image is subjected to histogram equalization to enhance the contrast of the image. Edge detection technique by the canny detector is applied for detection of the edges. Then any border of the image is removed. Further, the mathematical erosion and dilation are performed with the disk structuring element. By using threshold the microaneurysms are extracted. The images are compared by different performance measures and the values are tabulated in Table 1. In 5-level of wavelet decomposition the quantitative values, specificity and accuracy are higher for the $L5$ subband. For lower subbands these values are low.

Table 1. Performance measure values of extraction of microaneurysms in different level subbands in 5-level wavelet decomposition

Reconstructed image	SEN (%)	SPF (%)	SEB (%)	ACC (%)	EER (%)
L_1	79.96	62.80	37.20	63.42	18.29
L_2	62.78	58.45	41.55	58.47	20.76
L_3	63.08	73.71	26.29	73.22	13.39
L_4	60.61	76.63	23.37	75.90	12.05
L_5	59.28	**77.44**	22.56	76.65	11.67

Quantitative values (specificity and accuracy) are higher for the $L5$ wavelet subband. For lower subbands (i.e., $L2$), these values are found to be low. The accuracy value is found to be the highest for $L5$ subband, i.e., 76.65%. The value is the lowest in $L2$ subband, i.e., 58.47%. Equal error rate (ERR) is found to be the least, i.e., 11.67% for $L5$ subband. As the accuracy and specificity values are higher in $L5$ wavelet subband compared to the other subbands, it may be concluded that the microaneurysm information

in $L5$ subband is more. Thus, it is observed that the higher subband contributes more towards the microaneurysms information.

To study the variation of different performance measures across different images, boxplots for all subbands are shown in Figure 5. On each box, the central mark is the median, the edges of the box are the 25^{th} and 75^{th} percentiles, the whiskers extend to the most extreme data points the algorithm considers. The boxplots for specificity, accuracy, and equal error rate of sixty images for different wavelet subbands in 5-level wavelet decomposition are shown in Figure 5. From the boxplot, it is found that the average specificity and accuracy values for $L5$ subband are higher compared to the other subbands. For $L2$ subband, these values are the least. Thus, it can be concluded that more microaneurysm information is available in higher wavelet subband compared to the lower wavelet subband. The equal error rate is found to be the least in $L5$ subband.

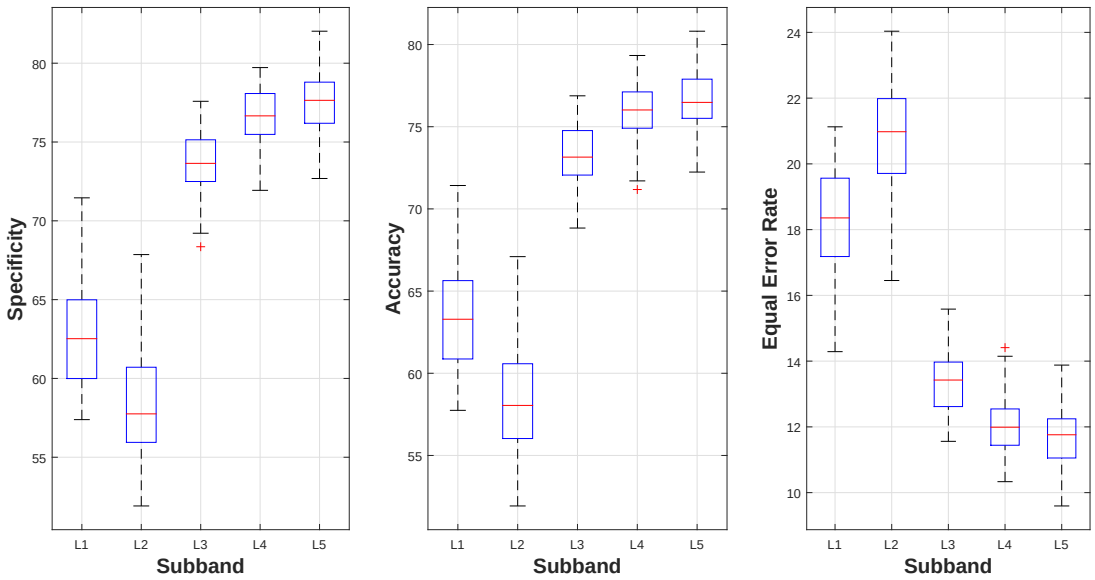

FIGURE 5. Boxplots for specificity, accuracy and equal error rate for different subbands in 5-level wavelet decomposition (by unaltering one subband coefficient at a time) for sixty images

Exudates are extracted from the original image and from the reconstructed images for different level decomposition and they are compared by the above-mentioned metrics to know the contribution of the different level subbands towards exudates information. Table 2 shows the performance measure values of the extraction of exudate features in different level subbands. In this table, L_1 to L_5 represent the reconstructed images by considering only one subband coefficients at a time, i.e., $L1$ to $L5$ subbands, respectively and the rest of the subbands coefficients are made zero. The reconstructed image L_1 contains the $L1$ subband coefficients only and all other level subband coefficients are altered and made to zero. From each reconstructed image the exudates are extracted for finding the contribution of subband coefficients towards exudates information. Similarly, 'Zero L_1' to 'Zero L_5' represent the reconstructed images by making $L1$ to $L5$ subband coefficients are zero, respectively and unaltering the other subband coefficients. In the reconstructed image 'Zero L_1', the coefficients of $L1$ subband are zero and the rest subband coefficients are present. Depending on the contribution of exudates for a particular subband, suitable subbands are combined to study the exudate information. For each case, the performance is calculated. The extraction of exudate in L_4 and L_5 reconstructed images provides higher accuracy. However, the extracted exudates in L_4 and L_5 reconstructed images

TABLE 2. Performance measure values of extraction of exudates in different level subband in 5-level wavelet decomposition

Reconstructed image	SEN (%)	SPF (%)	SEB (%)	ACC (%)	EER (%)	MSE	RMSE	PSNRv (dB)	MAE	PCC	UQI	SSIM
L_1	98.49	70.32	29.68	71.56	14.22	0.02	0.12	66.63	0.04	206852.10	0.59	1.00
L_2	98.64	70.62	29.38	71.86	14.07	0.01	0.12	66.70	0.04	208036.17	0.59	1.00
L_3	99.25	71.34	28.66	72.57	13.71	0.01	0.12	67.06	0.04	212871.51	0.59	1.00
L_4	99.54	71.21	28.79	72.46	13.77	0.01	0.11	67.49	0.03	217995.65	0.57	1.00
L_5	99.71	80.61	19.39	**81.47**	9.26	0.01	0.11	67.64	0.03	**218793.29**	0.66	1.00
Zero L_1	99.99	95.70	4.29	**95.90**	2.05	0.00	0.04	75.90	0.01	256179.68	0.90	1.00
Zero L_2	99.99	92.89	7.10	**93.22**	3.39	0.00	0.04	75.73	0.01	256006.03	0.84	1.00
Zero L_3	100	88.51	11.49	89.03	5.49	0.00	0.05	73.98	0.01	253085.33	0.76	1.00
Zero L_4	100	82.07	17.93	82.88	8.56	0.00	0.06	72.72	0.02	250233.77	0.69	1.00
Zero L_5	100	72.65	27.35	**73.85**	13.07	0.00	0.06	72.19	0.02	**248863.90**	0.62	1.00

highlight some blood vessels. Zeroing the $L1$ subband and $L2$ subband does not affect much in the accuracy for extraction of exudates, which are found to be 95.90% and 93.22%, respectively. The accuracy value is reduced to the lowest when $L5$ subband coefficients are made zero, which is found to be 73.85%. The structural changes are calculated by MSE, RMSE, PSNRv, PCC, UQI, and SSIM. Extraction of exudates in the reconstructed image L_5 provides higher PCC, ACC and SSIM measures. In L_5, only $L5$ subband information is present. Making the $L5$ subband coefficients zero, the performance values in the extraction of exudates reduce in the reconstructed image.

4. **Conclusions.** In this paper, diagnostic information (microaneurysms, hemorrhages, and exudates) of the fundus images is studied in different wavelet subbands for various levels of wavelet decomposition. The fundus image is decomposed into 3-, 5-, 7- and 9-levels by dB4 mother wavelet. From the above study, the following conclusions can be drawn.

In 3-level wavelet decomposition, all the subbands contribute equally to the diagnostic feature MAs. In 5-level wavelet decomposition subband $L1$, subband $L2$ and subband $L3$ contain less information about the MAs. Most of the diagnostic information is present in subband $L4$ and subband $L5$ in 5-level wavelet decomposition. So, during the analysis of microaneurysms, higher attention should be given to the coefficients of $L4$ and $L5$ subbands. In 7-level wavelet decomposition, $L5$, $L6$, and $L7$ contribute more information towards MAs. Subband $L5$ to subband $L9$ coefficients contain higher MAs information compared to other levels. Higher subband coefficients contain more MAs information compared to lower level subband coefficients. In 5-level wavelet decomposition subband $L1$, $L2$ do not contain much diagnostic information about exudates. The subbands $L4$ and $L5$ contain more blood vessel information. From the quantitative evaluation, it is found that $L5$ subband in 5-level wavelet decomposition contains higher exudate information. Combining the coefficients of subbands $L1$, $L2$, and $L3$ the exudate information can be preserved, and the blood vessel information can be suppressed. In 7-level wavelet decomposition subband $L1$, $L2$, $L3$, $L6$ and $L7$ contain the exudate information. The subbands $L2$, $L3$, and $L4$ do not contain significant information about the DR feature. In 9-level wavelet decomposition blood vessels information is present in $L4$ and $L5$ subbands.

The analysis presented in the work gives the diagnostic information in different wavelet subbands. It is observed that only a few subbands contain significant diagnostic information, and only such subbands are needed to be preserved for further analysis, storage, and transmission. This helps design computationally efficient classification techniques of the features which result in faster remote diagnosis. This method can also be extended for other medical images for analysis and remote diagnosis.

REFERENCES

[1] H. Safi, S. Safi, A. Hafezi-Moghadam and H. Ahmadieh, Early detection of diabetic retinopathy, *Survey of Ophthalmology*, vol.63, no.5, pp.601-608, 2018.

[2] S. Wild, G. Roglic, A. Green, R. Sicree and H. King, Global prevalence of diabetes: Estimates for the year 2000 and projections for 2030, *Diabetes Care*, vol.27, pp.1047-1053, 2004.

[3] J. Lechner, O. E. O'Leary and A. W. Stitt, The pathology associated with diabetic retinopathy, *Vision Research*, vol.139, pp.7-14, 2017.

[4] A. Sopharak, B. Uyyanonvara and S. Barmanemail, Simple hybrid method for fine microaneurysm detection from non-dilated diabetic retinopathy retinal images, *Computerized Medical Imaging and Graphics*, vol.37, nos.5-6, pp.394-402, 2013.

[5] W. Tasman and E. A. Jaeger, *Retinal Vascular Disease: Wills Eye Hospital Atlas of Clinical Ophthalmology*, 2nd Edition, Lippincott Williams and Wilkins Publication, 2001.

[6] T. A. Ciulla, A. G. Amador and B. Zinman, Diabetic retinopathy and diabetic macular edema, *Diabetes Care*, vol.26, no.9, pp.2653-2664, 2003.

[7] K. Yogesan, I. J. Constable, W. Morgan and D. Y. Soebadi, International transmission of teleophthalmology images, *Journal of Telemedicine and Telecare*, vol.6, pp.41-44, 2000.

[8] S. R. Nirmala, S. Dandapat and P. K. Bora, Wavelet weighted blood vessel distortion measure for retinal images, *Biomedical Signal Processing and Control*, vol.5, no.4, pp.282-291, 2010.

[9] M. K. Nath and S. Dandapat, Differential entropy in wavelet sub-band for assessment of glaucoma, *International Journal of Imaging Systems and Technology*, vol.22, no.3, pp.161-165, 2012.

[10] K. Udayakumar, P. P. Bharati, S. Verma and M. K. Nath, Automatic estimation of vision degradation from color fundus image, *I. J. Image, Graphics and Signal Processing*, vol.11, pp.26-34, 2015.

[11] S. Mallat, *A Wavelet Tour to Signal Processing*, 3rd Edition, Academic Press, Elsevier, 2009.

[12] Daubechies, *Ten Lectures on Wavelets*, SIAM, 1992.

[13] S. Lahmiri, Features extraction from high frequency domain for retina digital images classification, *Journal of Advances in Information Technology*, vol.4, no.4, pp.194-198, 2013.

[14] M. Niemeijer and B. V. Ginneken, *Drive Databse*, http://www.isi.uu.nl/Research/Databases/DRIVE /results.php, 2002.

[15] D. Farnell, *Aria Database*, www.eyecharity.com, 2010.

[16] Jean-Claude, *Messidor Database*, http://messidor.crihan.fr, 2010.

[17] A. Sopharak, B. Uyyanonvara, S. Barman and T. H. Williamson, Automatic detection of diabetic retinopathy exudates from non-dilated retinal images using mathematical morphology methods, *Computerized Medical Imaging and Graphics*, vol.32, no.8, pp.720-727, 2008.

[18] B. Antal and A. Hajdu, An ensemble-based system for microaneurysm detection and diabetic retinopathy grading, *IEEE Trans. Biomedical Engineering*, vol.59, no.6, pp.1720-1726, 2012.

[19] Z. Wang and A. C. Bovik, A universal image quality index, *IEEE Signal Processing Letters*, vol.9, no.3, pp.81-84, 2002.

[20] A. M. Mendonca and A. Campilho, Segmentation of retinal blood vessels by combining the detection of centerlines and morphological reconstruction, *IEEE Trans. Medical Imaging*, vol.25, no.9, pp.1200-1213, 2006.

[21] H.-H. Chang, A. H. Zhuang, D. J. Valentino and W.-C. Chu, Performance measure characterization for evaluating neuroimage segmentation algorithms, *NeuroImage*, vol.47, no.1, pp.122-135, 2009.

[22] C. Köse, U. Sevik, C. Ikibas and H. Erdol, Simple methods for segmentation and measurement of diabetic retinopathy lesions in retinal fundus images, *Computer Methods and Programs in Biomedicine*, vol.107, no.2, pp.274-293, 2012.

[23] A. M. Eskicioglu and P. S. Fisher, Image quality measures and their performance, *IEEE Trans. Communications*, vol.43, no.12, pp.2959-2965, 1995.

[24] A. M. Grigoryan and M. Grigoryan, *Brief Notes in Advanced DSP Fourier Analysis with MATLAB*, 1st Edition, Taylor and Francis, CRC Press, 2009.

[25] Z. Wang, A. C. Bovik, H. R. Sheikh and E. P. Simoncelli, Image quality assessment: From error visibility to structural similarity, *IEEE Trans. Image Processing*, vol.13, no.4, pp.600-612, 2004.

[26] D. Rousseau, A. Delahaies and Fran, Structural similarity measure to assess improvement by noise in nonlinear image transmission, *IEEE Signal Processing Letters*, vol.17, no.1, pp.36-39, 2010.